national accelerator laboratory NAL-Conf-73/67-THY/EXP
2000.000
7100.063

(Submitted to the Fifth International Conference
on High Energy Collisions, Stony Brook, NY,
August 1973)

REVIEW OF LARGE TRANSVERSE MOMENTUM PHENOMENA IN HADRON COLLISIONS

J. K. Walker

September 1973

Operated by Universities Research Association Inc. Under Contract with the United States Atomic Energy Commission

NAL-Conf-73/67-THY/EXP
2000.000
7100.063

REVIEW OF LARGE TRANSVERSE MOMENTUM PHENOMENA IN HADRON COLLISIONS

J. K. Walker
National Accelerator Laboratory, Batavia, Illinois 60510

ABSTRACT

Recent experimental data from NAL and the ISR on large transverse momentum single particle production in proton proton collisions are reviewed. The approach to energy scaling, particle ratios, and associated multiplicities, etc. are discussed.

INTRODUCTION

In the last year there has been a great deal of experimental and theoretical activity in the field of large transverse momentum phenomena. This activity was sparked by the striking experimental results of three groups,[1-3] at the ISR, reported at the Batavia Conference last year. They found that the pion production invariant cross section, which fell as $\exp(-6\,p_\perp)$ for $p_\perp < 1$ GeV/c, was many orders of magnitude above this function if extrapolated to $p_\perp$ of several GeV/c. Since that time, these groups from the ISR have reported new results and there is also new data from a group at NAL. This review will cover the data of these groups in order of increasing momentum transfer and/or increasing energy. Finally there will be some discussion[4] and interpretation of the data.

I. PHOTON AND HADRON PRODUCTION AT LARGE TRANSVERSE MOMENTUM

I.1 The NAL photon experiment[5] covers the energy range from 50 to 400 GeV. They have studied the reaction $p + p \rightarrow \gamma +$ "Anything" for gamma production at fixed angles in the laboratory. Figure 1 shows a schematic of the layout of their experiment. The circulating proton beam in the NAL accelerator performs multiple traversals through a gas or carbon filament target during the acceleration cycle. The data presented at this conference are for gamma production at a laboratory angle of 100 mrad. Data for 80 and 120 mrad are currently being analyzed. Figure 2 is a schematic

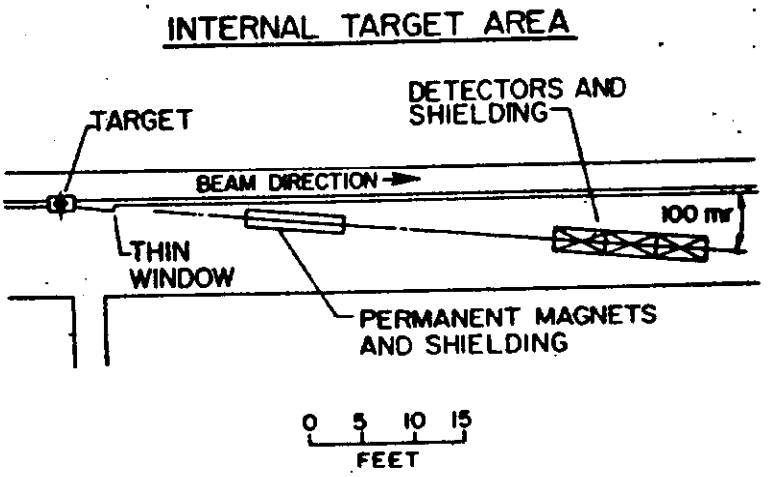

Fig. 1. Layout of the apparatus in the Internal Target Laboratory at NAL to study photon production in proton-proton collisions.

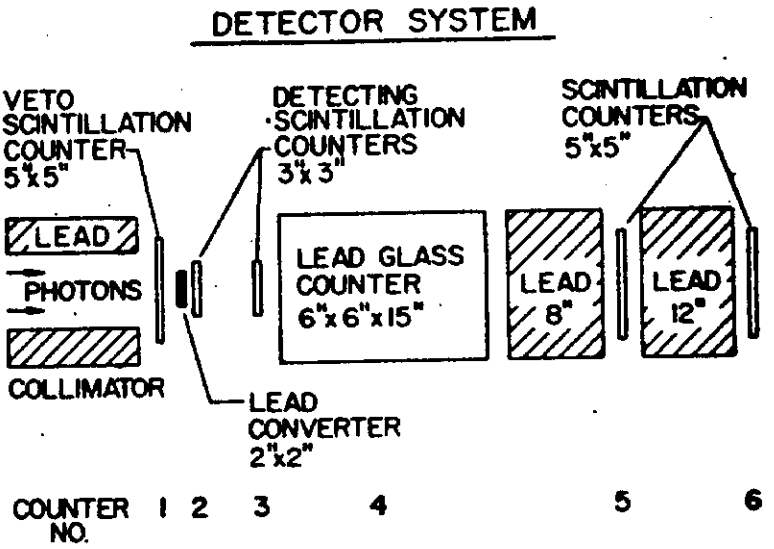

Fig. 2. Schematic of the photon detection apparatus.

of the apparatus. The solid angle of acceptance is 9.5 μsr. The lead converter is 1.1 radiation lengths and the lead glass counter had an effective length of 14 radiation lengths. The photon data are taken with a T, 2, 3, 4 trigger.

The events were divided into 25 GeV incident proton energy bins. A cut on the pulse height in trigger counter 2 required that events have a doubly ionizing or greater pulse height. An example of the

pulse height distribution of the lead glass counter is shown in Fig. 3

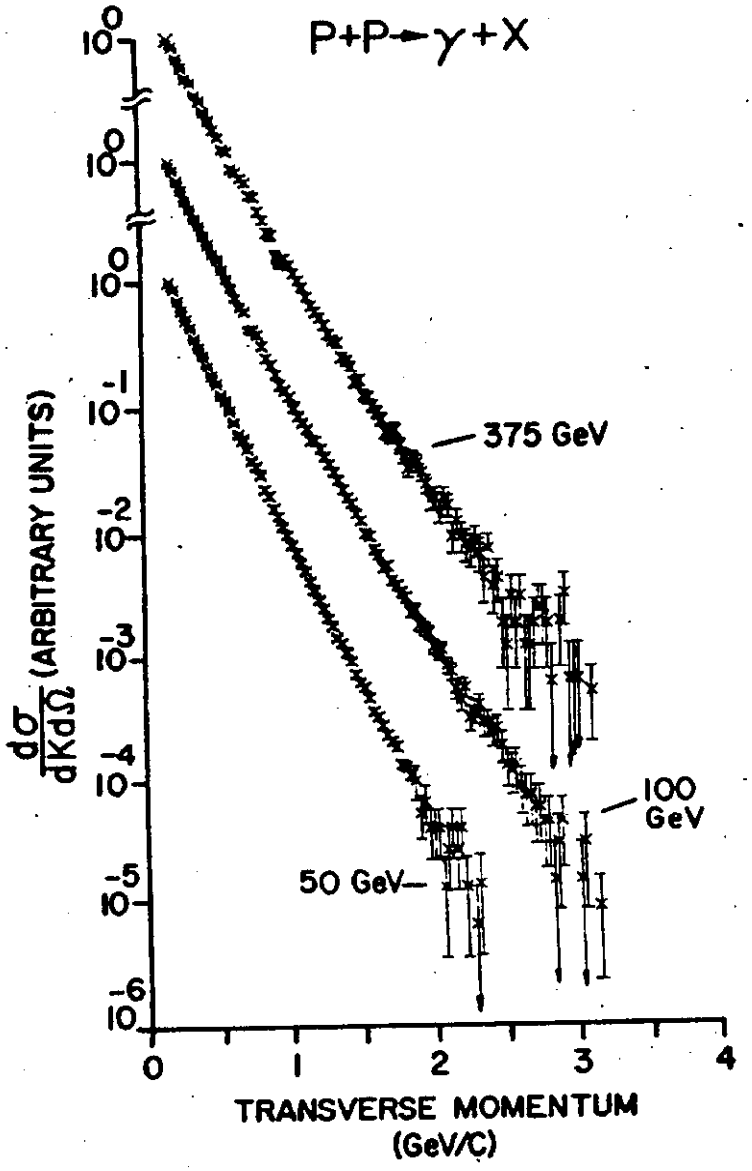

Fig. 3. Single photon inclusive cross section $d\sigma/d\Omega dk$ versus transverse momentum for 50, 100, and 375 GeV incident protons.

for proton energies of 50, 100, and 375 GeV. They have obtained data to a p_t between 3 and 4 GeV/c at each of 14 energies at each angle. The observed photon spectra were fitted with a function of the form

$$\frac{d\sigma_\gamma}{dp_\perp d\Omega} = A \exp(-Bp_\perp - Cp_\perp^2).$$

Figure 4 shows the results for B and C as a function of incident proton energy. There is excellent agreement between the hydrogen and

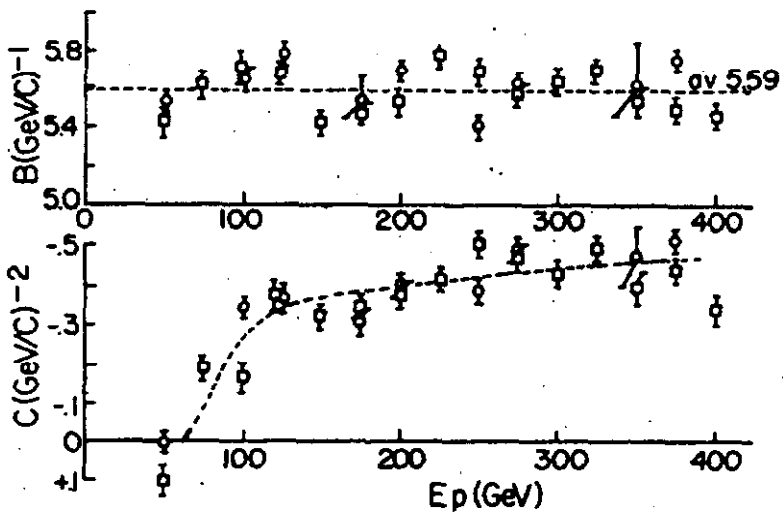

Fig. 4. Values of the parameters B and C for the photon cross sections. The circles and squares are for the hydrogen and carbon target data respectively.

carbon target data. The invariant inclusive π^0 cross section has been obtained from these photon data. A fit to the π^0 cross section with the same function as for the gamma data provides values for B and C within one standard deviation of the corresponding values for the photon data.

The results show the well known energy independence of the B parameter and the average value of B is given by

$$\langle B \rangle = 5.59 \pm 0.1.$$

The C parameter, on the other hand, starts out at zero then increases sharply between 50 and 125 GeV and varies rather slowly with further increase in energy. The importance of the C parameter is that it represents the deviation from a pure exponential $p_\perp$ distribution for the cross section. If indeed this result is confirmed by measurements at other angles,[6] which are currently being analyzed, then this is an extremely interesting conclusion. It is conceivable that the observed transition energy of about 100 GeV has something to do with the energy scale associated with the rising proton proton total cross section. The expression

$$\sigma_T = 38 + 0.68 \log^2 (\frac{E}{100}),$$

where E is the laboratory energy in GeV and σ is in millibarns reproduces the observed cross section from Serpukhov energies to the peak energy of the ISR. A possible connection of these two phenomena, that have an apparent energy scale of about 100 GeV, is of great importance. Of even greater significance is the underlying origin of this new energy scale.

I.2 The British-Scandinavian collaboration[7] have recently presented results on

a) the inclusive production of all charged particles at 90° and 59.4°,

b) particle ratios as a function of $p_\perp$.

Figure 5 shows the layout of the apparatus for the study of a) above.

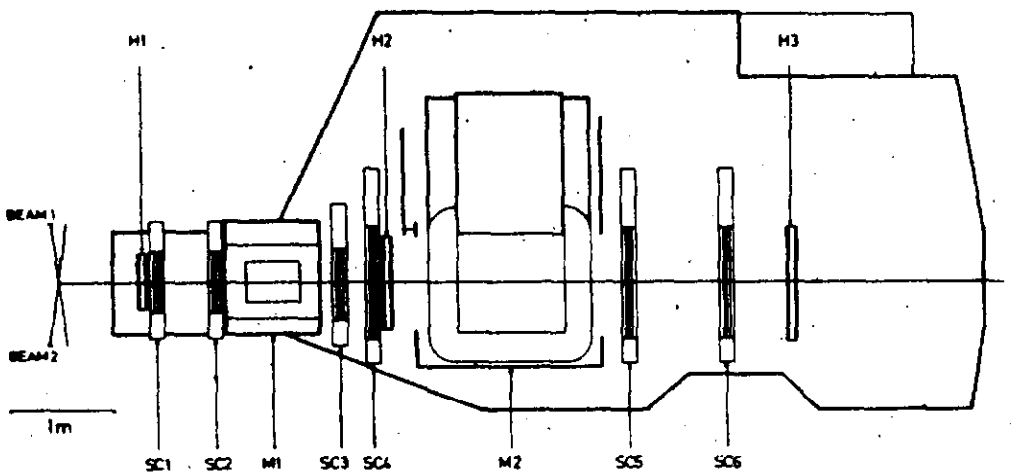

Fig. 5. Layout of the British-Scandinavian spectrometer at the ISR for the study of particle production at high transverse momentum.

The momentum of particles traversing the spectrometer is determined twice by deflection in the magnets M1 and M2. A trigger is formed by the coincidence of the three scintillation counter hodoscopes H1, H2, H3. The information from six spark chambers allows the path of the particle to be reconstructed and the particle momentum is obtained.

The resulting invariant cross sections $E\,d^3\sigma/dp^3$ for the inclusive production of positive and negative particles are shown in Fig. 6. The data are well represented as before by a function of the form:

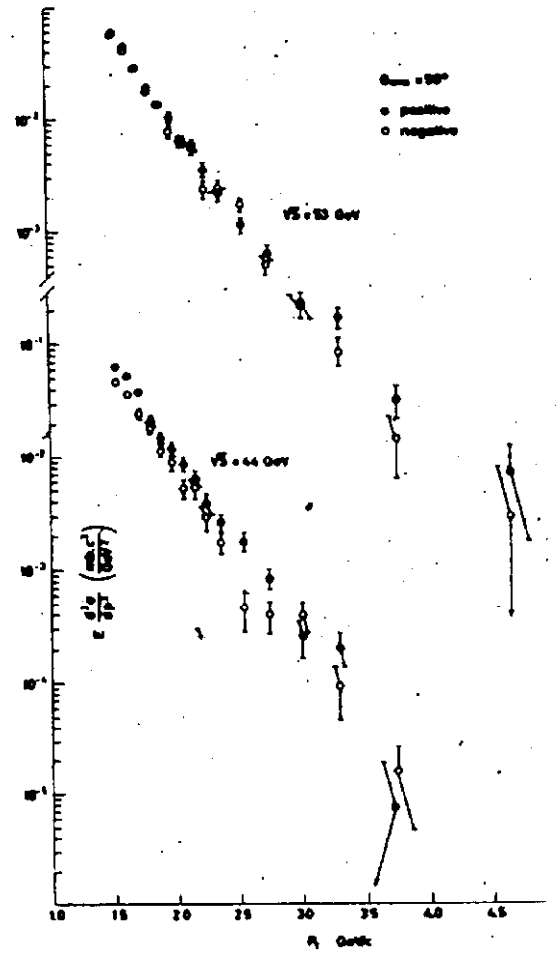

Fig. 6. Inclusive charge particle spectra at 90° in the center of mass for $\sqrt{s}$ = 44 and 53 GeV.

$$E d^3\sigma/dp^3 = Ae^{-Bp_\perp - Cp_\perp^2}$$

Little energy dependence is observed. This is probably due to the small range, $44 < \sqrt{s} < 53$, in center-of-mass energy.

We notice that the production of positive particles is larger than that of negative particles at medium $p_\perp$ even though at small $p_\perp$ ($<< 1$ GeV/c) they are approximately the same.

Similar results at an angle of 59.4° are shown in Fig. 7. An interesting aspect of these data is that the cross section, at 3 to 4 GeV/c transverse momentum, is the same at 90° and 59.4°. This corresponds to a range in x ($2p_\parallel/\sqrt{s}$) of about 0 to 0.1. Thus the well-known central plateau at low $p_\perp$ appears to exist at medium $p_\perp$ over at least the same and possibly larger range of x. It appears to be more appropriate (as at low $p_\perp$) to describe the large $p_\perp$ plateau in terms of rapidity or equivalently, the center-of-mass angle.

In the study of particle ratios, the spectrometer was modified to that shown in Fig. 8. The change was to remove one magnet and add two gas Cerenkov counters. Preliminary values for the particle ratio are presented in Fig. 9. The data show the striking feature that at $2 \leq p_\perp$ (GeV/c) ≤ 3.5, it is almost as frequent to find a heavy secondary as a pion. This has to be contrasted to what is found at low $p_\perp$ values, where pions dominate over heavy particles by a ratio close to 10.

Antideuteron production has been observed by the B.S. collaboration for the first time at the ISR. In the range $0.6 \lesssim p_\perp$(GeV/c) $\lesssim 1.0$. The invariant cross section can be parametrized as

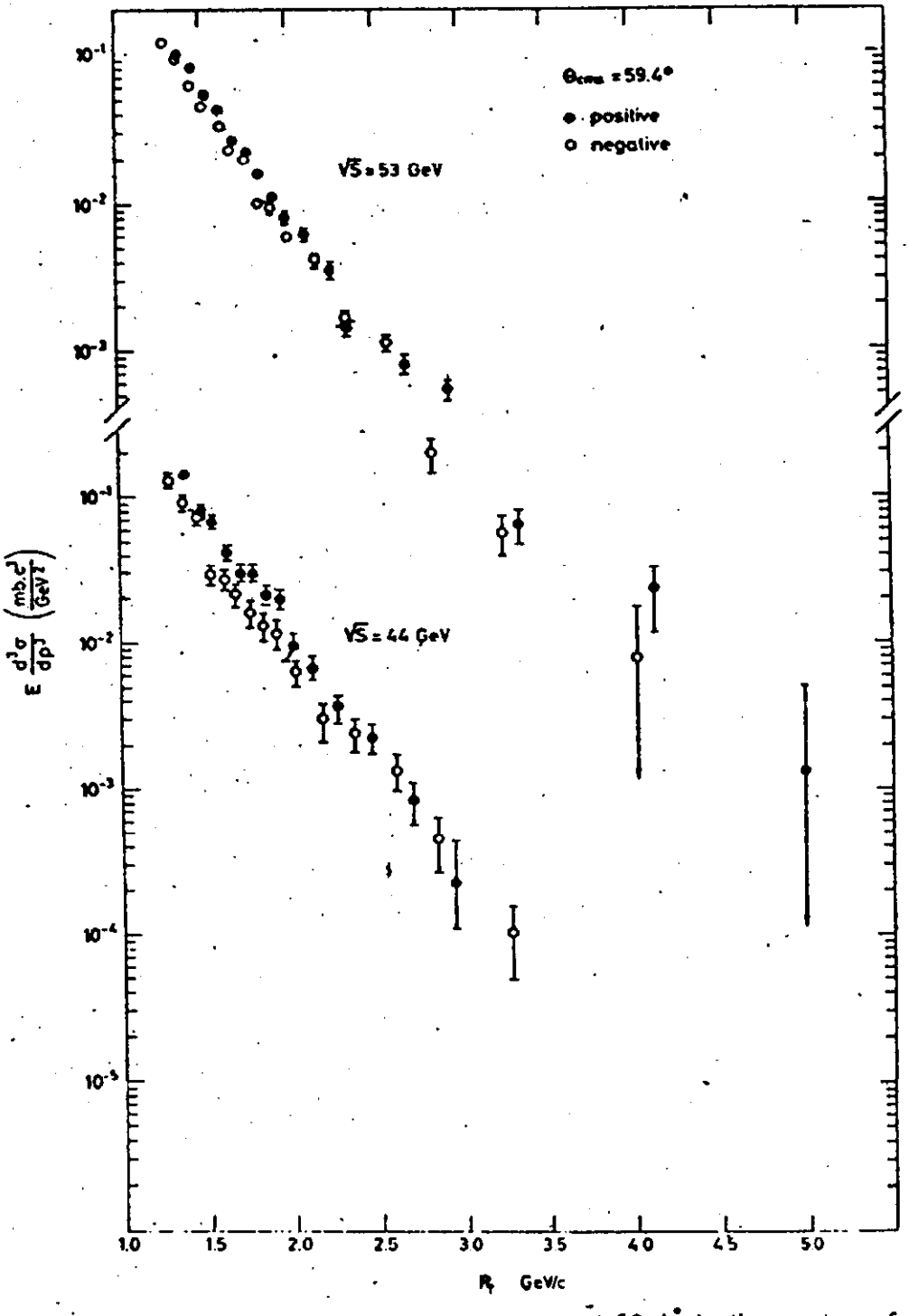

Fig. 7. Inclusive charge particle spectra at 59.4° in the center of mass for $\sqrt{s}$ = 44 and 53 GeV.

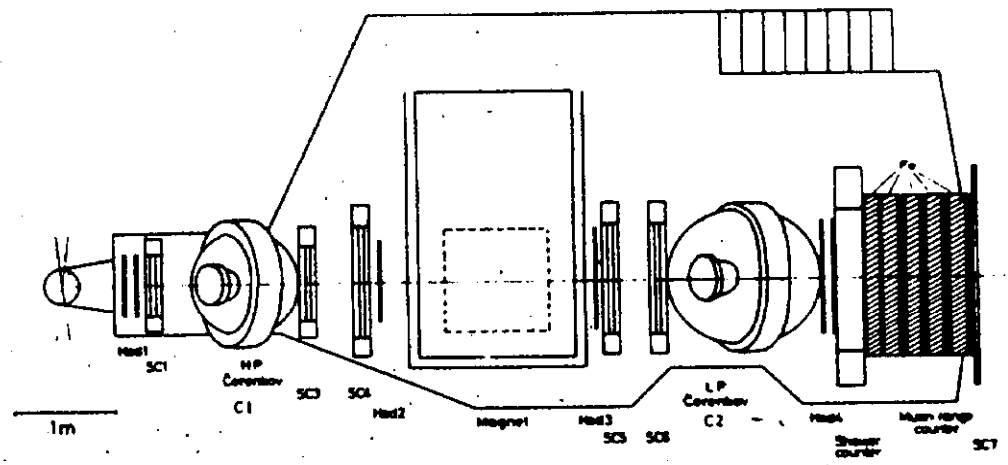

Fig. 8. Layout of the British-Scandinavian spectrometer at the ISR for the study of particle composition at intermediate transverse momentum.

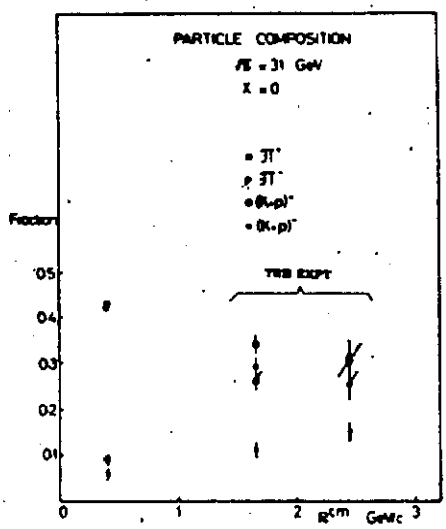

Fig. 9. Particle composition as a function of transverse momentum.

$$E\frac{d^3\sigma}{dp^3} = Ae^{-Bp_1},$$

where $A = 1.33\pm0.12\ \mu b \cdot c^3/GeV^2$

$B = 2.7\pm1.1\ (GeV/c)^{-1}$.

For comparison, they give the following ratios in the above momentum interval

$$\frac{Ed^3\sigma/dp^3 \,\big|\, \bar{p}}{Ed^3\sigma/dp^3 \,\big|\, \bar{D}_2} = (1.2\pm0.4)\times10^3.$$

Finally, deuteron production has been observed and they give a cross section production ratio of

$$\frac{\sigma \text{ deuteron}}{\sigma \text{ antideuteron}} = 3.5\pm1.5.$$

I.3 The Saclay-Strasbourg (S.S.) group[8] have obtained data for both gamma-ray and charged-particle production. Figure 10 shows

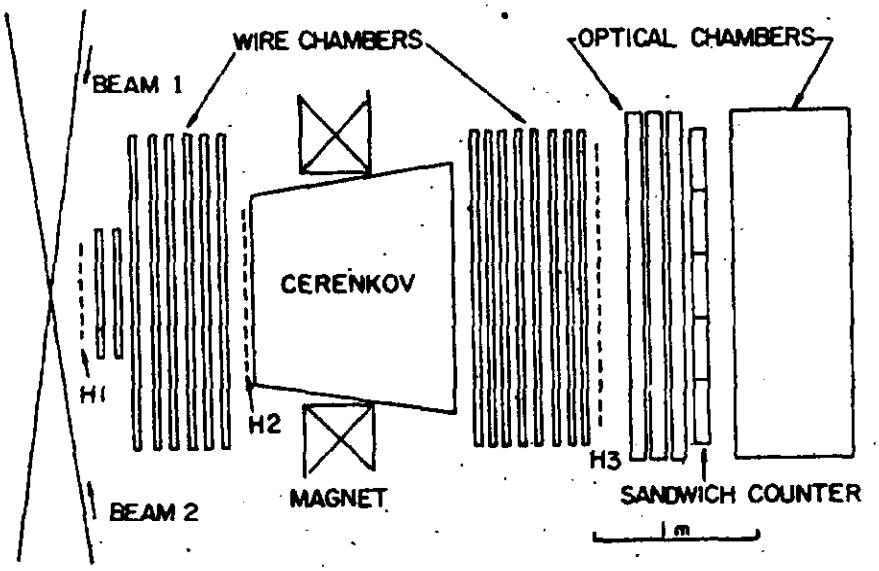

Fig. 10. Experimental layout of the Saclay-Strasbourg spectrometer at the ISR to study large transverse momentum particle production.

the layout of the apparatus. Counter hodoscopes H1, H2, and H3 were used to trigger on charged particles. Wire spark chambers were used to reconstruct trajectories and thereby obtain particle momenta. To measure cross sections above 2.8 GeV/c, a rejection against low transverse momentum is required. This is achieved in the trigger logic by requiring an output pulse from the Cerenkov counter.

Figure 11 shows the pion invariant cross section out to about a $p_\perp$ of 5 GeV/c. The exponential decrease has slowed down dramatically. In fact, for $3.5 \leq p_\perp \leq 5$ GeV/c the slope is $2.4 \pm 0.4\ (\text{GeV/c})^{-1}$ in sharp contrast with the slope $6\ (\text{GeV/c})^{-1}$ of the same spectrum below 1 GeV/c. Figure 12 shows the behavior of the invariant cross section at various $p_\perp$, with center-of-mass energy. The total negative cross section is always less than the total positive cross section. It should be observed that as $p_\perp$ is increased, the dependence on $\sqrt{s}$ is increased. To improve the statistical precision at the largest $p_\perp$ the quantity

$$\frac{1}{2} \int_{3.2}^{5.2} \left[\frac{d\sigma\pi^+}{dp_\perp d\Omega} + \frac{d\sigma\pi^-}{dp_\perp d\Omega} \right] dp_\perp$$

is plotted in Fig. 13. These data confirm the strong dependence of the cross section at large fixed $p_\perp$ on the center-of-mass energy.

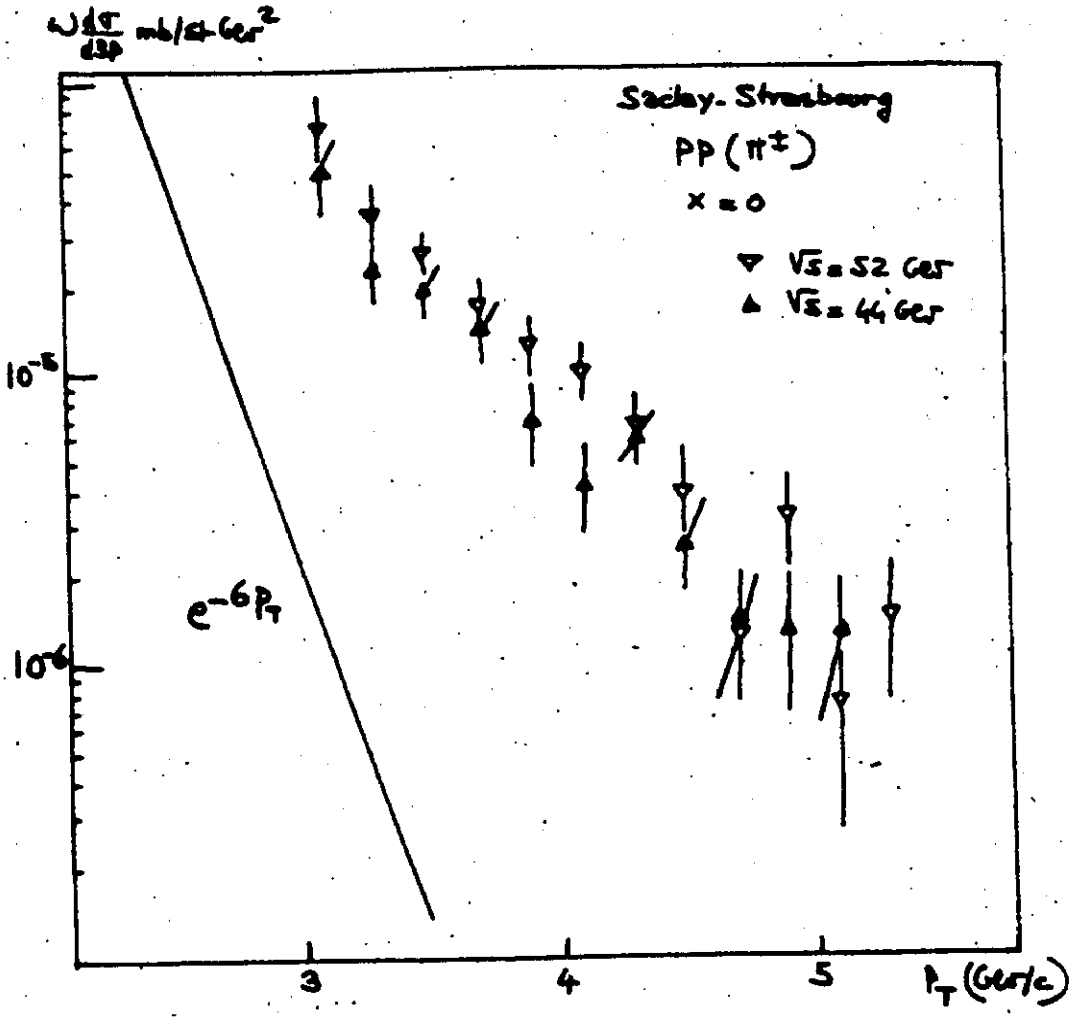

Fig. 11. Charged pion distribution at large $p_\perp$.

I.4 The CERN, Columbia, Rockefeller collaboration[9] have submitted to this Conference final results on inclusive π^0 production at large transverse momentum from proton-proton collisions at the ISR. It should be noted that all previous results reported by this group were for semi-inclusive cross sections.

Figure 14 shows a schematic of the apparatus which consisted of two identical spectrometers on the inner and outer sides of the colliding proton beams. Each spectrometer consisted of ten planes of wire spark chambers; four sets of scintillation counter hodoscopes A, B, Z, and ST; an array of 16 lead-glass counters, 3.1 radiation lengths thick; and an array of 60 lead-glass shower counters 14.8 radiation lengths thick. The A and B hodoscopes were used for

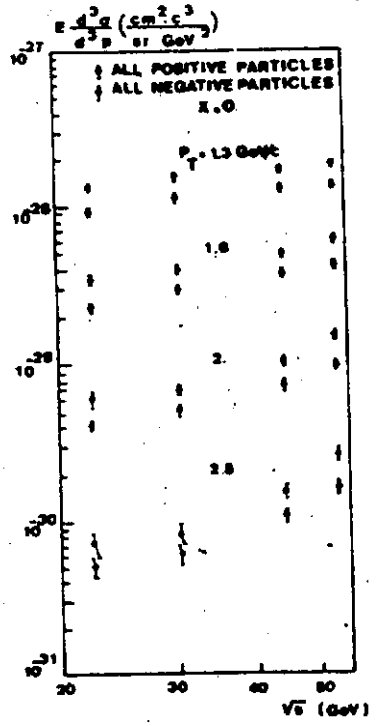

Fig. 12. Invariant charged pion cross sections at different $p_\perp$ as a function of center-of-mass energy.

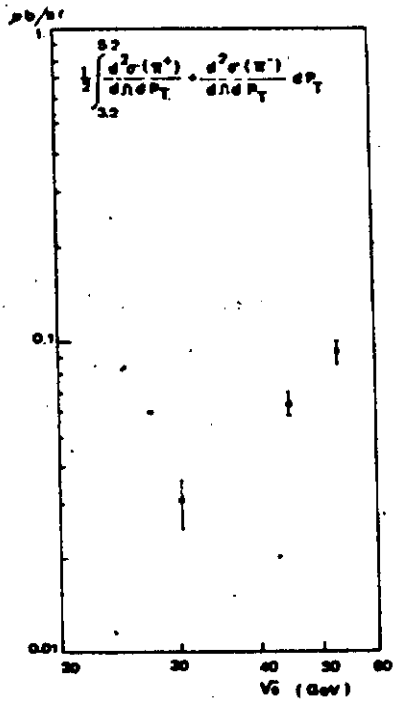

Fig. 13. Integrated pion yield $3.2 < p_\perp < 5.2$ GeV/c at 90° as a function of center-of-mass energy.

triggering. The Z counters were used to measure ionization loss and the ST counters were used for calibration purposes. For the data at $\sqrt{s}$ = 44.8 and 52.7 GeV, there was a 0.17-cm thick sheet of lead immediately preceding the Z counters of the inside spectrometer.

Independent of the spectrometers, there were two 1 m^2 scintillation counters, Σ_1 and Σ_2, centered around the downstream ISR vacuum pipes at a distance of 5.65 m from the intersection region. The coincidence $\Sigma_1\Sigma_2$ selected an almost pure sample of beam-beam collision events.

Two triggers were used in taking the data. When the lead sheet was in place the logic required a $\Sigma_1\Sigma_2$ coincidence. Otherwise, the logic required the presence of either a $\Sigma_1\Sigma_2$ coincidence or a coincidence between an A and B counter on the one side. An additional requirement in each trigger was a certain energy loss in both arrays of lead glass in one of the spectrometers.

Two methods were used to analyze the inside spectrometer data that were taken with the lead sheet in place. In the first approach

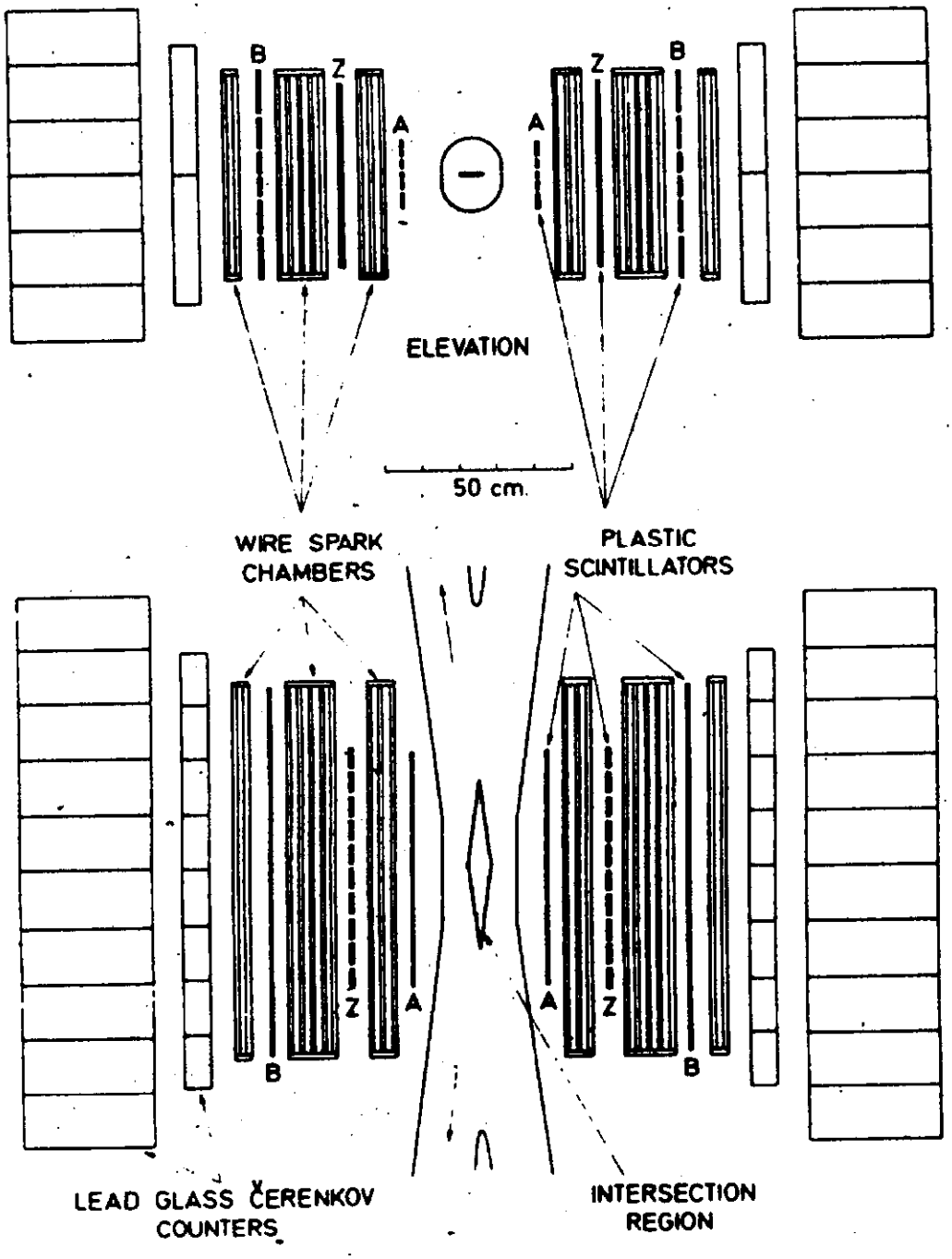

Fig. 14. Schematic of the CERN-Columbia-Rockefeller apparatus at the ISR.

only those events were selected, where, at least one photon was converted in the lead. The second method of analysis that was applied to all the data used only the energy loss in the lead glass counters.

To obtain inclusive cross sections it was necessary to know the triggering bias that resulted from the requirement of either the $\Sigma_1\Sigma_2$ coincidence or the detection of at least one track coming from the intersection region. This bias was deduced by dividing the data into three categories: 1) events with $\Sigma_1\Sigma_2$ and a track; 2) events with $\Sigma_1\Sigma_2$ and no track; 3) events with no $\Sigma_1\Sigma_2$ and a track. It was assumed that the observation of a track at large angles was independent of the presence of the $\Sigma_1\Sigma_2$ coincidence. This assumption allowed the estimation of the size of the undetected class of high $p_\perp$ events, in which there was no $\Sigma_1\Sigma_2$ coincidence or track. This correction was less than 50% at all energies and did not depend on $p_\perp$. For the data taken with the $\Sigma_1\Sigma_2$ trigger the corrections were slightly larger and $p_\perp$ dependent. There was reasonable agreement in these two methods of analysis.

Figure 15 shows the invariant π^o inclusive cross section as a function of transverse momentum for different center-of-mass energies.

An acceptable fit to the data for all energies can be made with the form

$$\frac{E d^3\sigma}{dp^3} = A \frac{1}{p_\perp{}^n} F(p_\perp/\sqrt{s}),$$

where $A = (1.54 \pm 0.1) \times 10^{-26}$

$n = 8.24 \pm 0.05$

and $F(p_\perp/\sqrt{s}) = \exp(-bp_\perp/\sqrt{s})$

where $b = 26.1 \pm 0.5$.

Because of systematic errors the data is consistent with $n = 8$.

A plot of the function $F(p_\perp/\sqrt{s})$ is shown in Fig. 16. This fit to the data leads to eventual scaling of the cross section at fixed $p_\perp$ for large enough s. To see this explicitly, Fig. 17 shows the extrapolated inclusive cross section at various center-of-mass energies up to and beyond that corresponding to a 1-TeV proton storage ring. It can be seen that at ISR energies the $p_\perp$ = 5 GeV/c and 10 GeV/c are respectively about a factor of 10 and 100 from their energy scaling limits. It appears that scaling is reached to a fair approximation even out at a $p_\perp$ = 25 GeV/c with a 1-TeV storage ring. Furthermore, since cross sections of 10^{-36} were measured with ISR luminosities it appears that momentum transfers in excess of 25 GeV/c can be measured with 1-TeV storage rings with luminosities a thousand times that of the ISR.

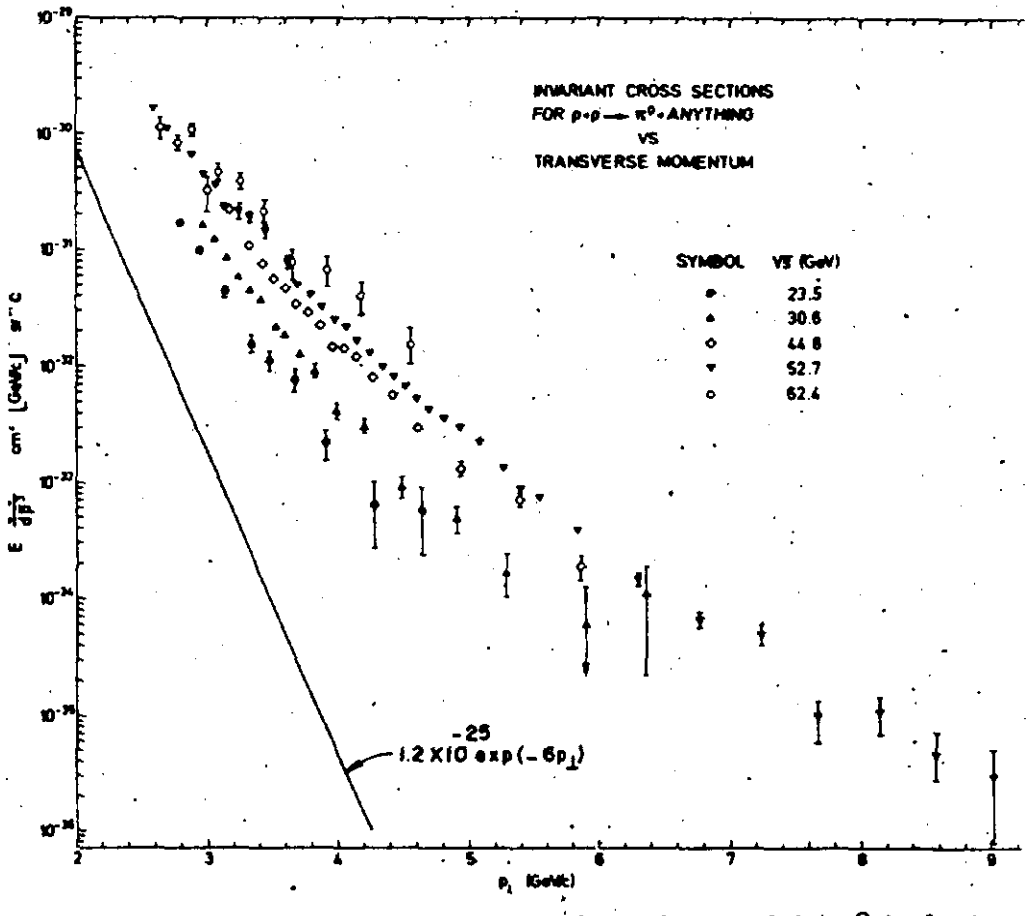

Fig. 15. The transverse momentum dependence of the π^0 inclusive invariant cross section at five center-of-mass energies. The errors are statistical only.

II. LEPTON PRODUCTION AT LARGE TRANSVERSE MOMENTUM

II.1 The CCR group also reported to this conference final results on their single and electron pair search. Single electrons of large transverse momentum would be expected from the decays of charged intermediate bosons, heavy leptons, or "charmed" particles. Electron pairs may arise from the production of time-like virtual photons, in proton-proton collisions, as well as from the decay of W^0's, heavy vector mesons, and Lee Wick heavy photons.

The apparatus used was identical to that already described and the triggers used were similar to those used in the π^0 experiment. The data for all experiments were recorded simultaneously.

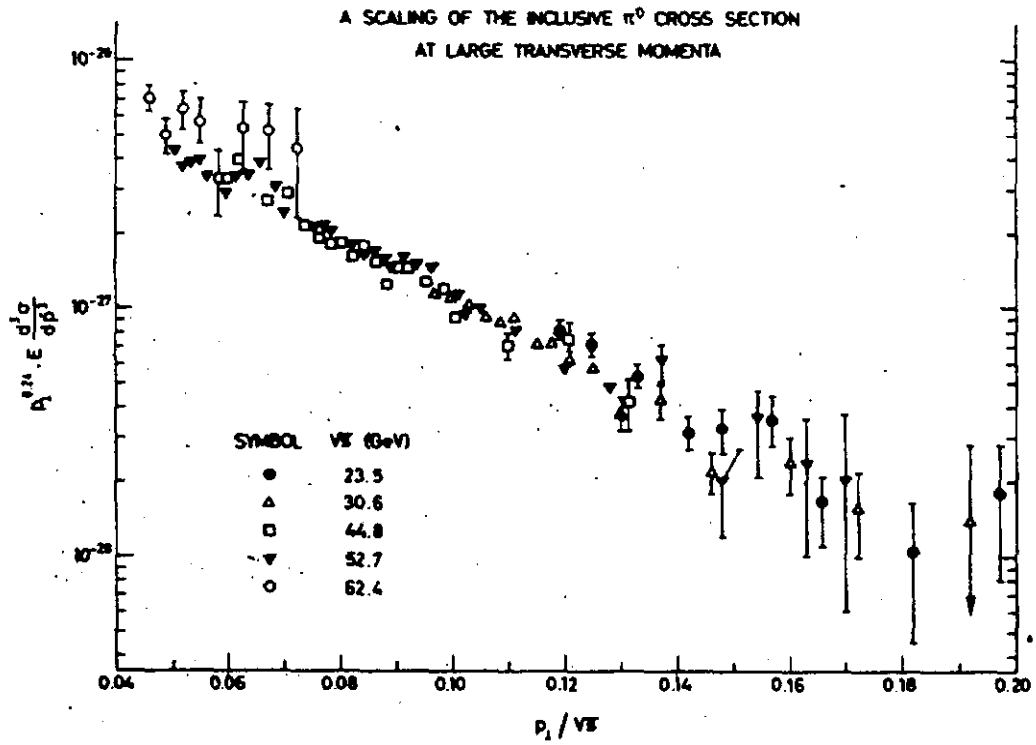

Fig. 16. The function $F(p_\perp/\sqrt{s}) = p_\perp^n E(d^3\sigma/dp^3)$, as deduced from the measurements, using the best fit value n = 8.24. The errors are statistical only.

The cross sections for single electron events are shown in Fig. 18 for the two spectrometers. For comparison, the observed π^0 spectrum is given. All spectra are parallel to one another. It is estimated that the background due to the chance overlap of a charged particle track and a π^0 within a single glass block is responsible for most, if not all, of the observed events. Hence, the cross sections are upper limits on the spectra of real electrons.

The electron-pair analysis yielded five events in which two tracks, on opposite sides of the apparatus, were found to satisfy the electron requirements. A study of background effects from $\pi^0\pi^0$ pairs simulating electron pairs gave an expected number of 4.6±0.5 consistent with zero pair signal.

The relationship between nondetection of electrons or electron pairs and an upper bound on the production of a massive parent state requires assumptions concerning the production and decay of the parent. Curve 1 of Fig. 19 shows the upper limit of the cross section for charged intermediate boson production obtained under the following assumptions:

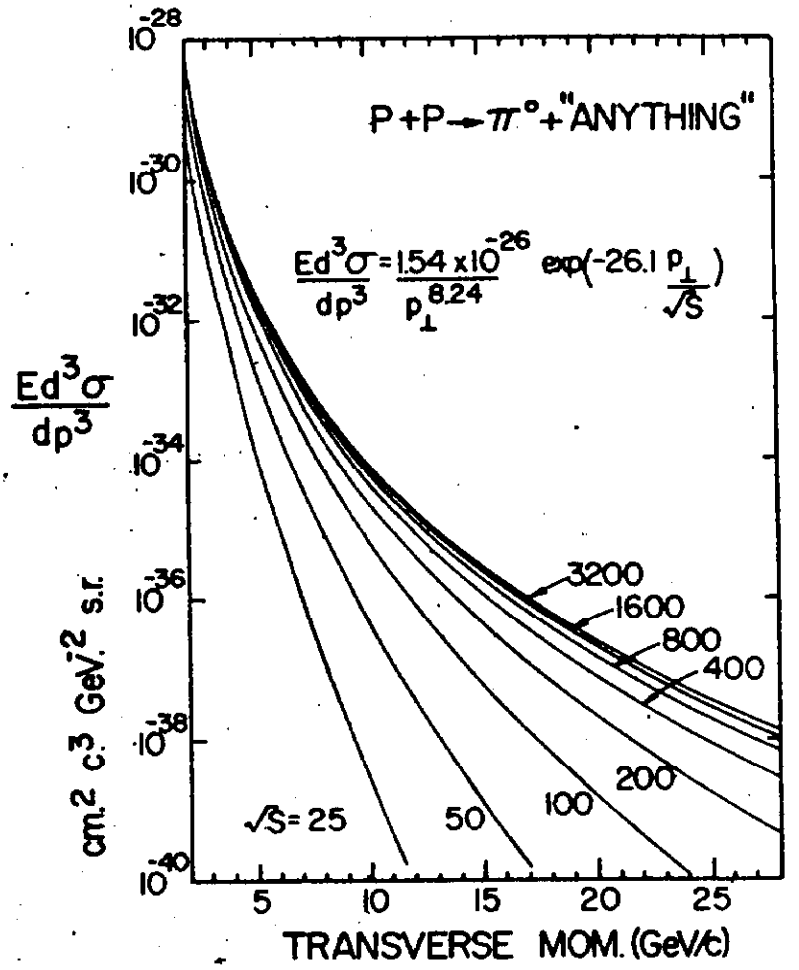

Fig. 17. The transverse momentum dependence of the π^0 inclusive invariant cross section at various center-of-mass energies using the CCR fitted function.

1) The W production distribution can be described by the parton-antiparton annihilation model of Drell and Yan.

2) The decay distribution is assumed isotropic.

3) The observed upper limit single electron spectra of Fig. 18 have been taken as an upper limit for masses below 15 GeV/c^2 and 95% confidence level has been taken for masses above 15 GeV/c^2 by the nonobservation of three events within a resolution bin.

For comparison purposes, curve 2 of Fig. 19 represents a possible lower bound prediction for charged W production based on the Drell-Yan model and CVC arguments. Under the assumptions of this model, it is possible to exclude the existence of charged W's with masses between 14 and 20 GeV/c^2.

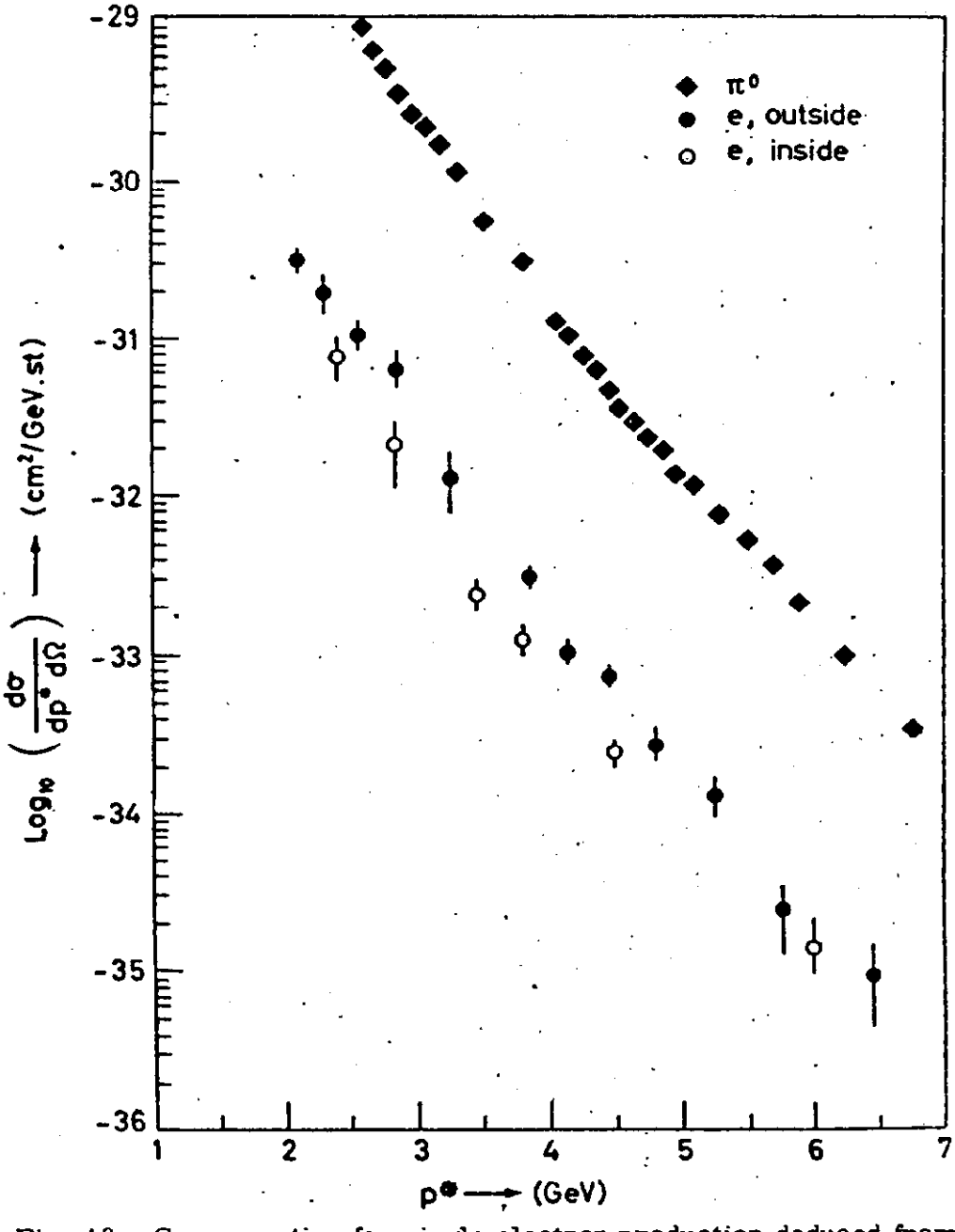

Fig. 18. Cross section for single electron production deduced from the two spectrometers. The π^0 cross section is also shown for comparison purposes.

Similar comparisons of the electron pair upper limit cross sections are made with models.

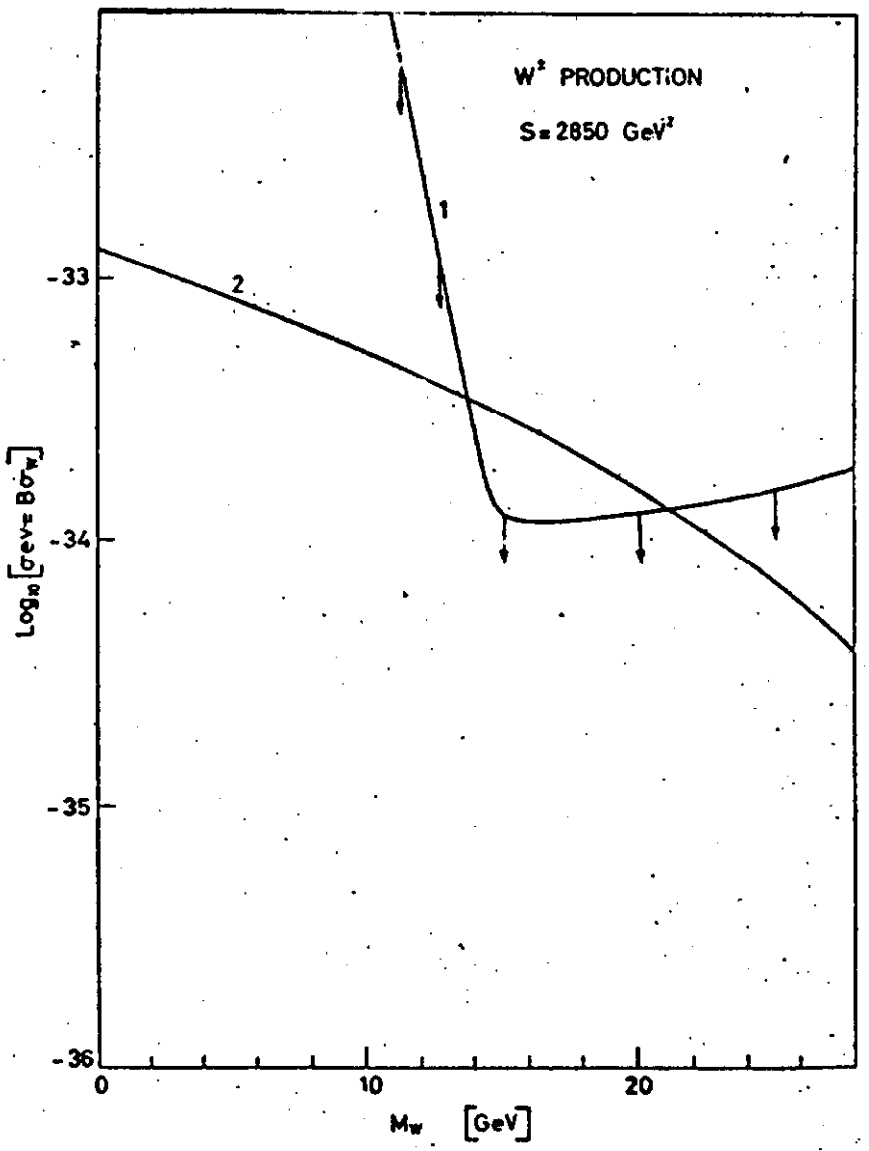

Fig. 19. Curve 1 is the cross section upper limit for charged intermediate bosons. Curve 2 is a possible lower bound prediction for charged intermediate boson production.

III. GENERAL CONSIDERATIONS

III.1 General Form of the Cross Section

Observation of appreciable cross sections at large momentum transfer did not come as a complete surprise![10,11] It is clear that

electromagnetic interactions should produce pions at large $p_\perp$, and in view of the SLAC results on deep inelastic electron scattering,[12] the pion yields should be expected to eventually drop with increasing $p_\perp$ as an inverse power only and nothing like the exponential dependence seen for $p_\perp \lesssim 1$ GeV/c. Pion production through the electromagnetic interaction could then be expected to become competitive with that resulting from purely hadronic phenomena at $p_\perp$'s about 5 GeV/c. In between 1 and 5 GeV/c there is nevertheless room for new possibilities to occur.

The striking results of all the experiments is that the pion yields at say $\geq$ 2 GeV/c are much larger than expected on the basis of extrapolating the exponential behavior found at < 1 GeV/c. The yield is very much larger than calculated from electromagnetic effects. Hence this new phenomenon is connected with the strong interaction of hadrons. It is clearly connected with very small distances inside the proton and hence is of fundamental importance to the nucleon structure.

For purely dimensional reasons we can express the invariant pion inclusive cross section for large $p_\perp$ in the form

$$E\frac{d^3\sigma}{dp^3} = \frac{1}{p_\perp^4} F\left(\frac{p_\perp}{\sqrt{s}}, y\right).$$

However, there is nothing to prevent us from multiplying this further by extra powers of $p_\perp$ associated with form factors, say

$$\left(\frac{m^2}{m^2 - p_\perp}\right)^p.$$

The function $F(p_\perp/\sqrt{s}, y)$ is a function of the dimensionless ratio $p_\perp/\sqrt{s}$ and the rapidity, y. In analogy to the deep inelastic structure function (νW_2, say) which shows a limiting behavior, it is reasonable to expect that $F(0,y) \to$ finite limit as $s \to \infty$ for fixed $p_\perp$. Thus we expect the yield for fixed large $p_\perp$ to scale eventually, but the more slowly the larger is $p_\perp$.

We therefore expect for the most general behavior of the cross section

$$E\frac{d^3\sigma}{dp^3} = \left(\frac{1}{p_\perp}\right)^n F\left(\frac{p_\perp}{\sqrt{s}}, y\right)$$

for $p_\perp >>$ any masses involved, say >> 1 GeV/c. Thus we expect an asymptotically scaling distribution that depends on an inverse power behavior of $p_\perp$. This kind of asymptotic expression can hold independently of the details of any specific model be it parton or modified multiperipheral.[13] However, it is generally agreed, that to the extent that the observed behavior reported by the CCR group

is described by an inverse power in $p_\perp (p_\perp^{-8})$ rather than an exponential dependence, there is some elementary particle (rather than Reggeon) exchange, or other point-like effect present.

III.2 Approach To An Energy Scaling Behavior

The CCR group have parametrized their data in the form

$$E \frac{d^3\sigma}{dp^3} = \frac{A}{p_\perp^{8.2}} \exp(-b\, p_\perp/\sqrt{s})$$

which leads to eventual energy scaling. However, it is possible to argue[14] that the observed s dependence is due to dynamical effects associated with the apparent point-like interactions which may not lead to eventual scaling. On the other hand, belated scaling is not "a priori" surprising. To illustrate this, Fig. 20 shows the plot of the π^0 fitted expression

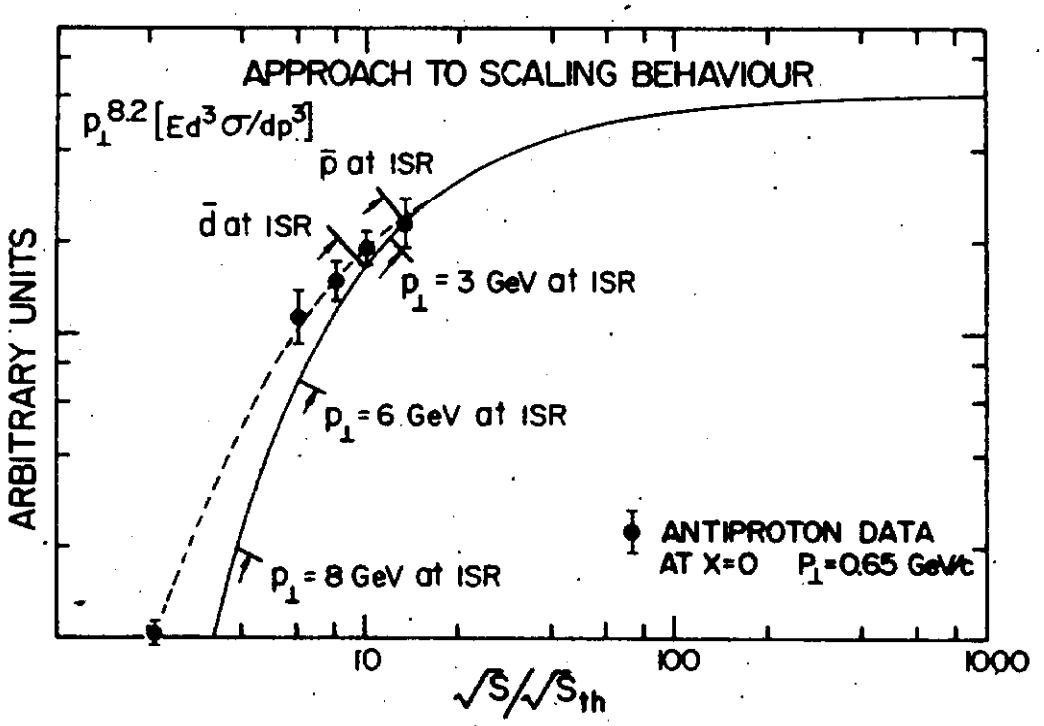

Fig. 20. The function $F(p_\perp/\sqrt{s}) = p_\perp^{8.2} E(d^3\sigma/dp^3)$ is shown as the solid curve versus $\sqrt{s}/\sqrt{s_{th}}$ where $\sqrt{s_{th}} = 2p_\perp$. The data points are for antiproton production and have been normalized to the curve at the highest energy. In this case $\sqrt{s_{th}}$ is the center-of-mass threshold energy for antiproton production. The dashed curve is a guide to the eye through the antiproton data points.

$$p_\perp^{8.2}\ E\frac{d^3\sigma}{dp_\perp^3} = A\exp(-b\,p_\perp/\sqrt{s})$$

versus $\sqrt{s}/\sqrt{s_{th}}$ where $\sqrt{s_{th}}$ is defined as the threshold center-of-mass energy for the production of a given large fixed $p_\perp$, i.e. $s_{th} = 4p_\perp^2$. In this way all π^o inclusive data lie on this universal approach to an energy scaling limit. Shown on the curve are various limits attainable for different $p_\perp$'s at ISR energies.

It is well known that the $\bar{p}$ cross section in the central region at the ISR has increased by a factor of 20 or so from 30 GeV. It is expected that the $\bar{p}$ cross section will eventually scale and that the present s dependence is most easily interpreted in terms of threshold effects. Plotted on Fig. 20 we show the available $\bar{p}$ data for the inclusive $\bar{p}$ cross section at $x = 0$ and small $p_\perp$ versus $\sqrt{s}/\sqrt{s_{th}}$ where $\sqrt{s_{th}}$ is defined as the threshold energy for $\bar{p}$ production. The $\bar{p}$ cross section at the highest s value has been arbitrarily normalized to the curve. It can be seen that the energy dependence of the inclusive data is quite similar to the $\bar{p}$ data. In addition, it suggests that the $\bar{p}$ cross section may rise perhaps by another factor of two or so if the comparison has any meaning. This is in reasonable agreement with the fact that the $p/\bar{p}$ ratio is about 2 and the proton cross section seems to be scaling already at ISR energies. Similar comparisons with antideuterons would be interesting. This comparison has not been intended to point out any deep connection between inclusive π^o production and $\bar{p}$ production but merely to emphasize that the observed strong s dependence of inclusive pion production at large $p_\perp$ is very likely to a large extent a threshold or kinematic effect. We certainly cannot rule out competing dynamical effects but it is going to be extremely difficult to demonstrate their presence.

III.3 Charge Effects

At low $p_\perp$ (< 0.6 GeV/c) most secondaries are pions and there are as many π^+ as π^- produced at peak ISR energies. As the momentum transfer is increased a positive excess appears. The Saclay-Strasbourg results shown in Fig. 12 indicate that the positive to negative yield for $2 < p_\perp < 3.5$ GeV/c is about 1.5. Clearly in the kinematic limit of large $p_\perp$ the positive to negative yield goes to infinity. Much more data at larger $p_\perp$ and over a range of s is required to begin to sort out the meaning of the excess positive to negative yield.

It is interesting that the quark parton model[15] leads to a positive to negative yield of about 2 in the scaling limit. This is related to the ratio of u to d quarks in the proton.

III.4 Particle Ratios

Figure 9 shows the British-Scandinavian collaboration results for particle ratios in the range $1.4 < p_\perp < 3.5$ GeV/c. There is a rather dramatic effect as noted earlier in that the pions have lost the overwhelming majority that they enjoyed at low $p_\perp$. Much more data on particle ratios should shortly be available from NAL and the ISR.

In the meantime it is worth speculating on some possible behaviors of particle ratios at intermediate to large momentum transfer. It is reasonable to assume that the general form,

$$E\frac{d^3\sigma_\pi}{dp^3} = \left(\frac{1}{p_\perp}\right)^{N_\pi} F_\pi\left(\frac{p_\perp}{\sqrt{s}}, y\right)$$

which has been found to be applicable to pions will also be applicable for kaons and baryons. In these cases, however, it is important at intermediate momentum transfers (say $\lesssim$ 4 GeV/c) to attempt to take into account mass effects. A natural attempt in this direction[16] is to substitute $\sqrt{p_\perp^2 + m^2}$ for $p_\perp$. In this way, we obtain for baryon production:

$$E\frac{d^3\sigma_B}{dp^3} = \left(\frac{1}{\sqrt{p_\perp^2 + M_B^2}}\right)^{N_B} F_B\left(\frac{\sqrt{p_\perp^2 + M_B^2}}{\sqrt{s}}, y\right).$$

For simplicity we take the same functional form of F_B as found for pions at $y = 0$, namely

$$F_B = A_B \exp\left(-b_N\sqrt{p_\perp^2 + M_B^2}/\sqrt{s}\right).$$

We may take $A_B/A_\pi = 1$ as it does not affect the variation of the fraction of baryons to pions as a function of momentum transfer.

For fixed center-of-mass energy there are therefore two parameters N_B and b_N (we know $N_\pi = 8$ and $b_\pi = 26$) which control the fraction of baryons to pions as a function of $p_\perp$. We may spectulate on possible ranges of values of these two parameters:

(i) On the general basis that the nucleon form factor goes as $1/t^2$ while the pion form factor is thought to go as $1/t$ it is likely that $N_B \geq N_\pi$.

(ii) Also, on the general grounds that the approach to energy scaling for baryons is expected to be as slow or slower than for pions it is likely that $b_N \geq b_\pi$. (In our previous discussion of approach to energy scaling behavior it appeared that $b_N \geq b_\pi$.).

As a result, if any one of the following three conditions is satisfied:

The increase in R up to the maximum at $p_\perp \approx 3$ GeV/c is due entirely to the mass term in $(1/\sqrt{p_\perp^2 + M_B^2})^{N_B}$. The fall off in R at $p_\perp > 3$ GeV/c is due to the assumption $N_B > N_\pi$ or $b_N > b_\pi$. These two possibilities can be distinguished by a quite different dependence of R on center-of-mass energy, $\sqrt{s}$, as seen in Fig. 21.

Similar remarks can be made about the kaon to pion ratio as a function of transverse momentum. In this case the maximum in the ratio occurs at $p_\perp \sim 1.5$ to 2 GeV/c. It will be extremely interesting to see if these general expectations are confirmed by measurements in the very near future.

We need to accumulate a body of data at various $p_\perp$ and over as wide a range of energy as possible to begin to extract the general trends of the particle ratios. Our main purpose in this discussion has been to emphasize the expected importance of kinematic effects.

III.5 Associated Multiplicity

Triggering on a large transverse momentum secondary, one may measure the associated multiplicity within a neighboring region of phase space and compare it to the average value. Since the production of a large $p_\perp$ secondary takes a good fraction of the center-of-mass energy, which is left over by leading particle effects, one would think that such a configuration would have to be associated with a relatively low mean multiplicity. The opposite result occurs. It appears that a trigger on a large $p_\perp$ secondary is a bias in favor of a large associated multiplicity. The multiplicity excess appears to be located at similar rapidities. Furthermore, there is evidence that the multiplicity not only exceeds average in the direction of the detected particle, but also in the direction opposite. So far the data is very limited. However, the CCR collaboration have reported the number of charged tracks within limited solid angles associated with a π^0 with various $p_\perp (x_\perp = 2p_\perp/\sqrt{s})$. Figures 22 and 23 show the associated mean number of tracks in the case of the "jet" opposite the detected π^0 and the "jet" in which the π^0 is detected. These results have to be compared with the rate observed for "typical" events defined in terms of a beam-beam interaction $\Sigma_1\Sigma_2$ trigger. Typically there is a factor of about two enhancement in the associated multiplicities for the case of the large $p_\perp$ trigger. The curves in Figs. 22 and 23 are the results of fits to the data by Ellis and Kislinger using a parton model.[15] It appears that the general features of the data are inherent in any simple parton model. The extent to which there are kinematic correlations which could, independently of parton effects, produce these results is not clear. However, it seems unlikely that kinematics alone could account for these large effects observed in the associated multiplicities.

a) $N_B > N_\pi$; $b_N = b_\pi$
b) $N_B = N_\pi$; $b_N > b_\pi$
c) $N_B > N_\pi$; $b_N > b_\pi$

then an interesting and rather general behavior of the ratio R is obtained, where

$$R = \frac{Ed^3\sigma_B/dp^3}{Ed^3\sigma_\pi/dp^3}.$$

First, R will increase as a function of $p_\perp$ out to about $p_\perp \approx 3$ GeV/c as observed by the British-Scandinavian collaboration. Beyond $p_\perp \approx 3$ GeV/c, however, R will then decrease as $p_\perp$ is increased further. It is intriguing that no data exist beyond $p_\perp \approx 3$ GeV/c to see the predicted maximum in R.

Figure 21 shows possible behaviors of R for the two cases a) and b) above. The existence of a maximum in R at about $p_\perp \approx 3$ GeV/c is not very sensitive to the choice of parameters.

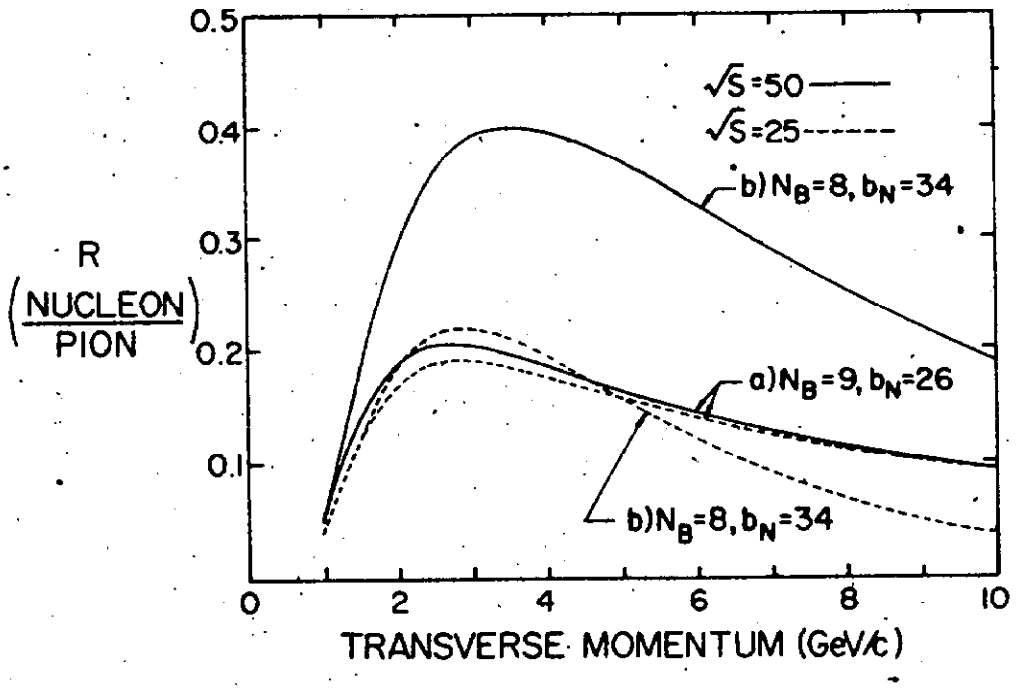

Fig. 21. The predicted general form of the baryon to pion ratio of inclusive cross sections at large momentum transfer. The different curves are for two different values of the parameters N_B and b_N at two different center-of-mass energies.

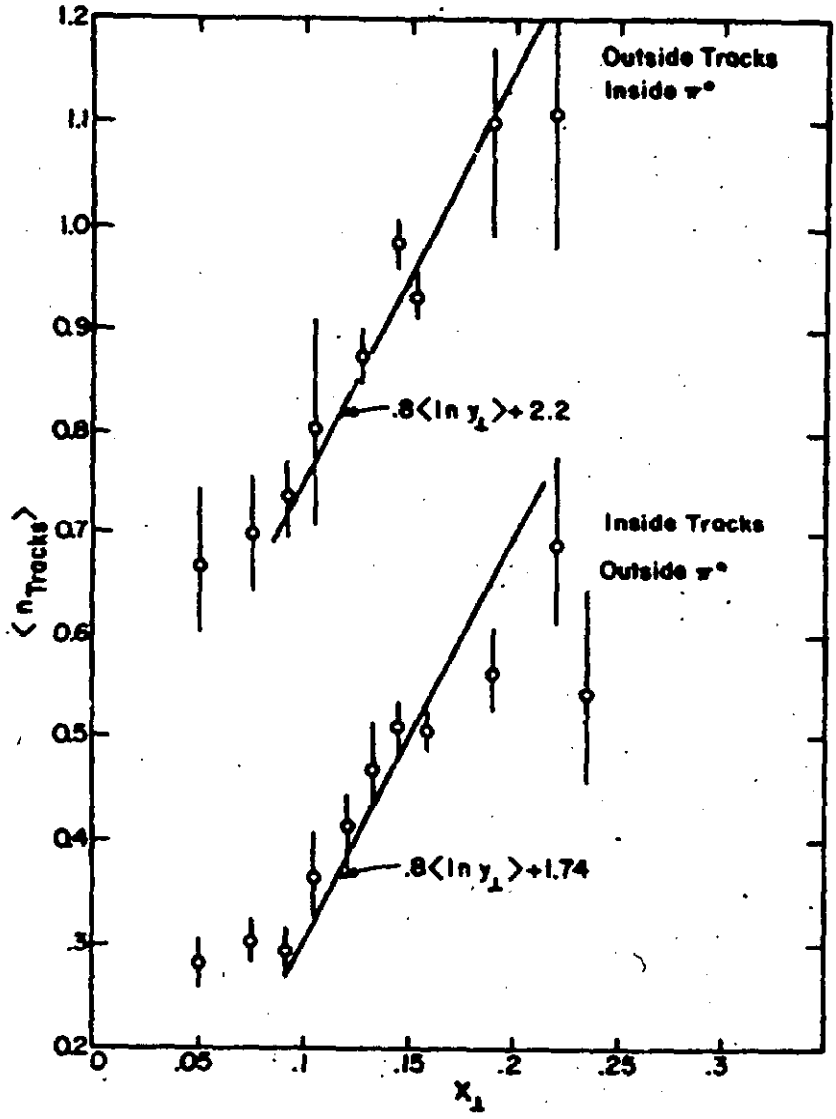

Fig. 22. The associated mean charged track multiplicity of the "jet" opposite the detected π^0 as a function of π^0 normalized transverse momentum. The curves are predictions of a parton model.

Several new experiments at the ISR, by the new SS-CCR setup, the streamer chamber and the split field magnet program should shed light on the question of associated multiplicities.

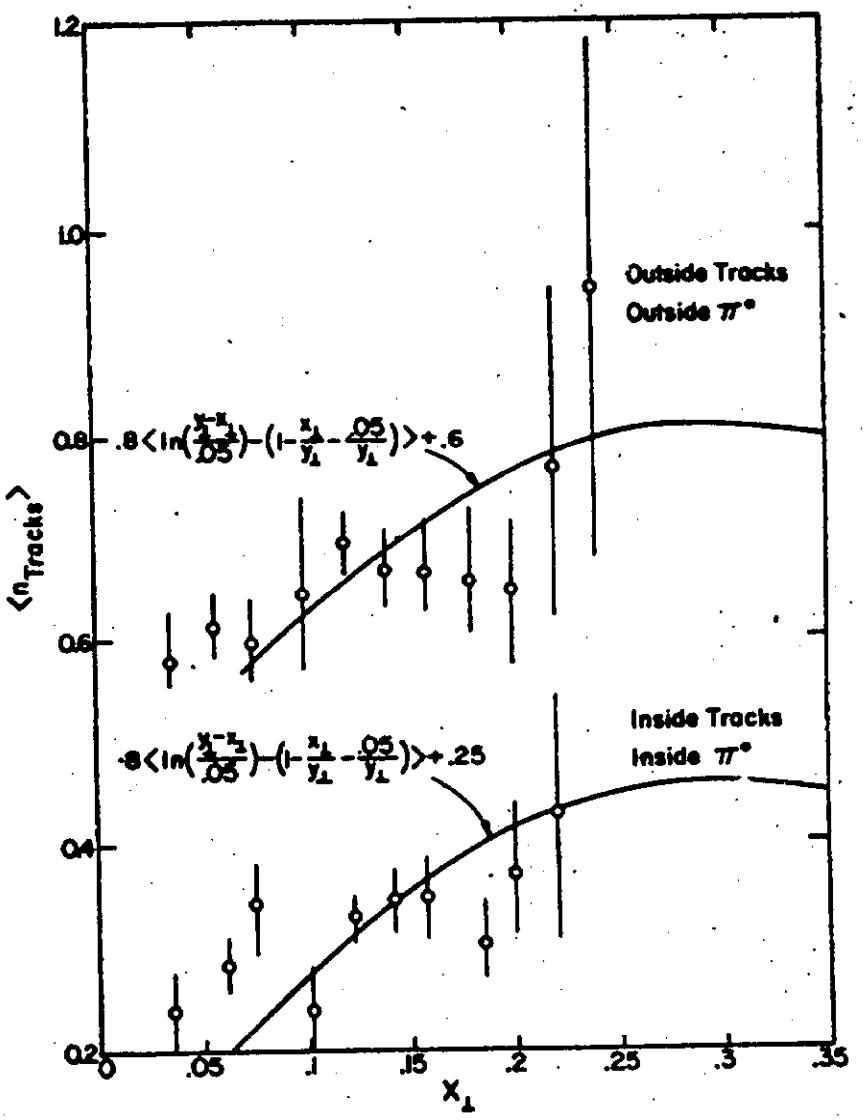

Fig. 23. The associated mean charged track multiplicity of the "jet" in the same direction as the detected π^o as a function of π^o normalized transverse momentum. The curves are predictions of a parton model.

IV. OTHER HADRON-INITIATED REACTIONS

The experimental study of large $p_\perp$ secondaries initiated by incident beams with different quantum numbers promises to be a rich tool to investigate the qualitative features of these phenomena. As an

example along these lines, the predictions are given in Table I of a quark parton model with vector gluon exchange. The expected particle ratios are given for some different projectiles and target combinations. The production of very intense pion beams and a program to begin to study these possibilities is under consideration at NAL at this time.

CONCLUSIONS

A totally new field in hadron physics has opened up within the last year in the study of large transverse momentum phenomena. We are certainly not in a dull asymptotic energy domain but rather in a region where there are rapid energy dependencies and where there are qualitatively new features appearing. It is likely that there are further surprises in store for the second generation of experiments in this developing field. Although a very high energy proton storage ring, of even modest luminosity, would clarify the existence of jets and their properties, the use of secondary beams at several hundred GeV may also provide an important qualitative handle in this study.

ACKNOWLEDGMENTS

I thank my colleagues for numerous interesting discussions, especially J. Johnson and F. Taylor. In addition, I have benefitted from stimulating discussions with M. Einhorn, S. Ellis, T. T. Wu, L. Lederman, R. Cool, J. Cronin, H. Boggild and S. Brodsky.

REFERENCES

1. CERN-Columbia-Rockefeller collaboration, paper submitted to the XVI International Conference on High Energy Physics, Chicago and Batavia, September, 1972.
2. Saclay-Strasbourg collaboration, paper presented at the XVI International Conference on High Energy Physics, Chicago and Batavia, September, 1972.
3. British-Scandinavian collaboration, paper presented at the XVI International Conference on High Energy Physics, Chicago and Batavia, September, 1972.
4. A good general discussion of new experimental results from the ISR has recently been given by M. Jacob, CERN TH.1683. A much more complete list of references is given therein.
5. D. C. Carey et al., paper submitted to this conference.
6. It should be pointed out that for photon detection at fixed angle in the laboratory, there is a connection between the corresponding center-of-mass angle, θ, and s.

Therefore, an alternative explanation of the behavior of the C parameter is its possible dependence on θ. Measurements at different angles will separate the θ and s dependence of C.

7. B. Alper et al., Phys. Letters 44B, 521 (1973); B. Alper et al., Phys. Letters 44B, 527 (1973).
8. M. Banner et al., Phys. Letters 44B, 537 (1973).
9. CERN-Columbia-Rockefeller collaboration, paper submitted to Phys. Letters.
10. S. Berman et al., Phys. Rev. D4, 3388 (1971).
11. F. Low and S. Treiman, Phys. Rev. D5, 756 (1972).
12. For a review of deep inelastic electron scattering see F. Gilman, Physics Reports 3C, 542 (1972).
13. D. Amati et al., CERN preprint (1972).
14. D. Cline et al., University of Wisconsin preprint (1973).
15. S. D. Ellis and M. B. Kislinger, NAL preprint NAL-Pub-73/40-THY (1973).
16. Various authors have considered inserting mass terms in somewhat similar fashion to reproduce π/K production ratios at low $p_\perp$ and in other reactions where SU(3) symmetry is badly violated. An example along these lines is R. C. Arnold, ANL/HEP 7125 (1971).

Table I. Naive Limiting Charged Multiplicity Ratios ($s \to \infty$, x non-wee, $\langle \epsilon \rangle << 1$) According to the Parton Model of Ref. 15.

Process	$\frac{\langle \pi^+ + \pi^- \rangle}{2\langle \pi^0 \rangle}$	$\frac{\langle \pi^+ \rangle}{\langle \pi^- \rangle} - \frac{\langle K^+ \rangle}{\langle K^0 \rangle}$	$\frac{\langle K^+ \rangle}{\langle K^- \rangle}$	$\frac{\langle K^0 \rangle}{\langle \bar{K}^0 \rangle}$	$\frac{\langle K^+ + K^0 \rangle}{\langle K^- + K^0 \rangle}$
pp	1	2(2.4)	>> 1	>> 1	>> 1
pn	1	1	>> 1	>> 1	>> 1
$\pi^+ p$	1	5(6.6)	>> 1	2/3	3(4.7)
πn	1	$\frac{1}{5}(\frac{1}{6.6})$	2/3	>> 1	3(4.7)
$\pi^- p$	1	$\frac{1}{2}(\frac{1}{2.4})$	4/3	>> 1	3(3.5)
$\pi^+ n$	1	2(2.4)	>> 1	4/3	3(3.5)